Editors' Suggestion

Direct Atomic-Scale Observation of Ultrasmall Ag Nanowires that Exhibit fcc, bcc, and hcp Structures under Bending

Shiduo Sun,[1,*] Dongwei Li,[1,*] Chenpeng Yang,[1] Libo Fu,[1] Deli Kong,[1] Yan Lu,[1] Yizhong Guo,[1] Danmin Liu,[1] Pengfei Guan,[2] Ze Zhang,[3] Jianghua Chen,[4] Wenquan Ming,[4] Lihua Wang,[1,†] and Xiaodong Han[1,‡]

[1]*Institute of Microstructure and Property of Advanced Materials, Beijing Key Lab of Microstructure and Property of Advanced Materials, Beijing University of Technology, Beijing 100124, China*

[2]*Beijing Computational Science Research Center, Beijing 100084, China*

[3]*Department of Materials Science, Zhejiang University, Hangzhou 310027, China*

[4]*Center for High-Resolution Electron Microscopy, College of Materials Science and Engineering, Hunan University, Changsha, Hunan 410082, China*

(Received 24 May 2021; revised 23 September 2021; accepted 22 November 2021; published 3 January 2022)

Metals usually have three crystal structures: face-centered cubic (fcc), body-centered cubic (bcc), and hexagonal-close packed (hcp) structures. Typically, metals exhibit only one of these structures at room temperature. Mechanical processing can cause phase transition in metals, however, metals that exhibit all the three crystal structures have rarely been approached, even when hydrostatic pressure or shock conditions are applied. Here, through *in situ* observation of the atomic-scale bending and tensile process of ~5 nm-sized Ag nanowires (NWs), we show that bending is an effective method to facilitate fcc-structured Ag to access all the above-mentioned structures. The process of transitioning the fcc structure into a bcc structure, then into an hcp structure, and finally into a re-oriented fcc structure under bending has been witnessed in its entirety. This re-oriented fcc structure is twin-related to the matrix, which leads to twin nucleation without the need for partial dislocation activities. The results of this study advance our understanding of the deformation mechanism of small-sized fcc metals.

DOI: 10.1103/PhysRevLett.128.015701

It is well established that metals usually have one of three crystal structures: face-centered cubic (fcc), body-centered cubic (bcc), or hexagonal-close packed (hcp). Because the structures of metals can significantly affect their properties [1,2], finding an efficient method that can access all three of these structures of a given metal and reveal the atomistic mechanisms of phase transition among them is greatly desired in metal science and technology research. Such a method would provide scientific guidance for the synthesis of metals with desired properties. Although all three of these crystal structures can be accessed by phase transitions from the liquid phase through solidification, most metals normally exhibit only one stable structure at room temperature [3]. Owing to the importance of phase transitions, they have been extensively studied for decades [4,5]. For instance, mechanical processing can transform a metal from one stable structure to another [6,7]. However, metals that can access all three structures are rare because phase transition requires a very complicated stress state [4,5]; furthermore, the process is always disrupted by inevitable dislocation and twinning mechanisms [8–19]. Previous molecular dynamics (MD) simulations predicted that ultrasmall-sized metals can access two of the above-mentioned structures at room temperature [20–23] because small nanowires (NWs) can suppress dislocations and twinning, which facilitates deformation governed by structural transition. This prediction was further confirmed by several experiments on fcc metals several nanometers in size [9,10,19,24]. For example, Zheng *et al.* observed the transformation of fcc Au into a bcc structure at the crack tip of an Au nanocrystal [19]. Wang and coworkers also revealed that small-sized fcc Au nanocrystals transformed into a bcc structure during necking [25]. Although these results show that several nanometer-sized fcc metals can indeed experience fcc–bcc phase transition, only transitions between these two crystal structures were accessed at room temperature through deformation [9,10,19,24]. Previous studies have also shown that fcc-hcp transformation occurs in small-sized Ag during shock loading or under ultrahigh pressure (>8 GPa) [26–28]. Under complicated stress conditions, such as ball milling and compression, hcp-fcc and fcc-hcp phase transitions were observed in hcp Hf and fcc CrCoNi films, respectively [29,30]. These studies show that in extremely high or complicated stress states, fcc metals can usually access only two crystal structures. Even under extreme conditions such as shock and hydrostatic pressure [26–28], fcc, bcc, and hcp structures have rarely been simultaneously accessed at room temperature. It is still unclear whether all three structures can be realized via the mechanical processing of a given metal. Thus, an

efficient method that can access all the structures of a given metal at room temperature, and confirm their formation via *in situ* atomic-scale experiments, would be of interest.

Using a homemade *in situ* deformation device (see Supplemental Material for details [31–33]), the atomic-scale deformation behavior of Ag NWs with diameters of ~5 nm was captured *in situ* using spherical aberration-corrected transmission electron microscopy (Cs-TEM). The results revealed that applying bending strain is an effective method for fcc-structured Ag to access bcc and hcp structures. The tensile plastic strain was governed by partial dislocations, resulting in stacking faults and deformation twins. Our results provide an efficient method for fcc-structured metals to access three structures at room temperature.

Figure 1 shows a sequence of Cs-TEM images that were captured along the $[1\bar{1}0]$ zone axis, which show the atomic-scale bending process of a single-crystalline Ag NW. Fast Fourier transform (FFT) of the images corresponding to the blue-framed region are shown in the inset. As shown in Fig. 1(a), the NW exhibits an axial direction of [001] and a diameter of ~5 nm; it can also be observed that the single-crystal NW contains no dislocations. The FFT image indicates that the root of the NW is an fcc structure. As shown in Figs. 1(c) and 1(c), as the bending strain was increased, a bcc lattice was observed at the bottom of the NW, which was confirmed by the FFT image of the red-framed region. As can be seen from the FFT image in Fig. 1(c), the spots can be well indexed with bcc Ag. With an increase in the bending strain, as shown in Fig. 1(d), many of the bcc lattices further transformed into hcp. As can be seen from the FFT image, the spots can be well indexed with hcp Ag. By comparing the area of the phase transition region in Figs. 1(d) and 1(e), it can be observed that these newly formed phases underwent growth process as the bending strain increased, and three types of phases, i.e., fcc, bcc, and hcp, were observed. With further bending, the bcc and hcp lattices transformed into a re-oriented fcc phase [Fig. 1(e)]. It is worth noting that the re-oriented fcc structure is twin-related to the matrix; the twin boundary (TB) is indicated by the red dashed line. In our bending experiments, the fcc, bcc, and hcp phases were consistently observed (also see other examples in Figs. S1–S3 [31]), indicating that bending is an effective method for fcc-structured metals to access all three structures at room temperature.

To reveal the bending-induced phase transition more clearly, Figs. 2(a)–2(c) show three enlarged ⟨110⟩ Cs-TEM images. By comparing these images, it can be seen that the lattice shape and spacing at the bottom region of the NW is different from that of the fcc lattice. Since the imaging condition of our *in situ* Cs-TEM images was unchanged, this implies that the change in the lattice shape and spacing should be directly related with the structural change. As shown in Fig. 2(a), a bcc lattice was observed in the compressive region of the Ag NW. Upon carefully checking the lattices, the angle between the (111) and $(11\bar{1})$ planes was observed to have decreased from ~109° to 90°, which is consistent with the measured bending angle of the NW (as shown in Fig. S4 [31]). The relationship between the fcc and bcc structures is consistent with the Bain transformation path (Fig. S5, Tables I–III [31]). With an increase in bending strain, as shown in Fig. 2(b), both the bcc and hcp lattices were frequently observed (also see Figs. S1–S3 [31]). The relationship between bcc and hcp is shown in Fig. S6 and Tables I–III. [31] With further straining, the hcp and bcc phases in the compressive region transformed back into fcc phases [Fig. 2(c)], leading to

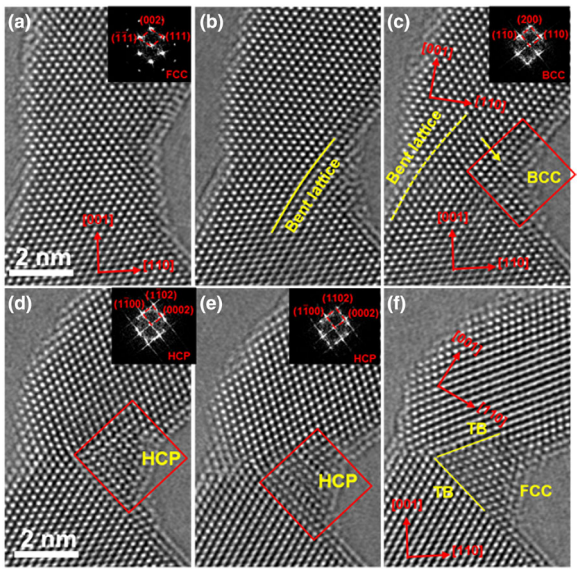

FIG. 1. *In situ* Cs-TEM images along the fcc $[1\bar{1}0]$ zone axis showing the bending process of a ~5 nm-sized Ag NW. The inset image shows the corresponding FFT pattern of the blue-framed region.

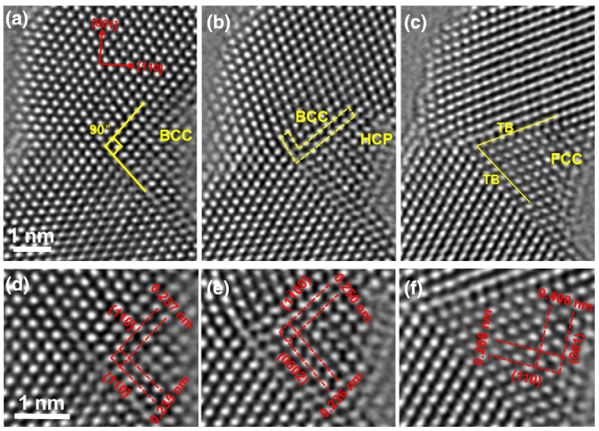

FIG. 2. (a)–(c) Enlarged Cs-TEM images showing the fcc-bcc-hcp-fcc phase transformation at the bottom of the NW during bending. (d)–(e) The corresponding enlarged Cs-TEM images of (a)–(c) show the bcc, hcp, and fcc phases in detail.

region III becoming a twin with regions I and II [Fig. 2(c)]. Figures 2(d)–2(f) show enlarged Cs-TEM images corresponding to the red-framed region of Figs. 2(a)–2(c), respectively. As indicated by the red dashed line in Fig. 2(d), the lattice in this region exhibits a square shape, and the spacings of the lattice planes are 0.236 and 0.235 nm. These parameters can be well calibrated by the {110} plane of bcc Ag viewed along the [100] zone axis ($a = b = c = 0.333$ nm), which was confirmed by *ab initio* simulation (see Fig. 3). As indicated in Fig. 2(e), in the hcp lattice region, the measured spacings of the lattice planes were 0.250 and 0.235 nm. The interplanar angles and spacing cannot be calibrated by fcc-structured Ag but can be well calibrated by the $\{1\bar{1}00\}$ and (0002) planes of hcp Ag viewed along the $[11\bar{2}0]$ zone axis ($a = b =$ 0.293 nm and $c = 0.479$ nm) [39], which was also confirmed by *ab initio* simulation (see Fig. 3). With further bending, this region transformed into a re-oriented fcc lattice. As shown in Fig. 2(f), the lattice spacing is consistent with fcc Ag with $a = b = c = 4.08$ Å. This re-oriented fcc lattice structure is twin-related to the matrix, which contradicts the wide belief that deformation twining occurs via partial dislocation mechanisms. The bent strain can lead to the local structure varying slightly from the ideal fcc lattice; thus, the contrast in the Cs-TEM image is slightly displaced.

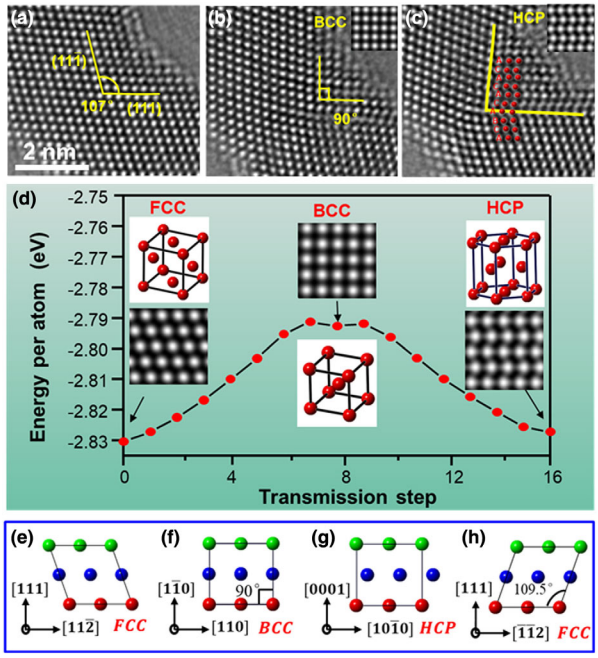

FIG. 3. Enlarged Cs-TEM images and atomic model showing the fcc-bcc-hcp-fcc phase transformation path. (a)–(c) The crystal lattice between the (111) and $(11\bar{1})$ planes changes from the original fcc to a bcc and then to an hcp lattice. The inset in (b),(c) show simulated images of bcc- and hcp-structured Ag. (d) Calculated energy curves of the fcc-hcp phase transition through the bcc path. The inset in (d) shows simulated HRTEM images of fcc-, bcc-, and hcp-structured Ag and the corresponding 3D models. (e)–(h) 2D models of fcc-, bcc-, and hcp-structured Ag.

Figures 3(a)–3(c) show three enlarged Cs-TEM images of the bottom of the Ag NW depicting the phase transition process during bending. Before the phase transition [Fig. 3(a)], the angle between the (111) and $(11\bar{1})$ planes was ~107° (this angle for an ideal fcc lattice is 109.5°), indicating that the fcc lattice was subjected to a large strain without any dislocation activity. In Fig. 3(b), two types of fcc and bcc phases of Ag are shown. As shown in Fig. 3(c), many of the bcc lattices transformed into hcp lattices. Thus, three types of phases, i.e., fcc, bcc, and hcp, were observed in Ag NWs. This indicates that the fcc–hcp transition, which follows an fcc-bcc-hcp path, likely occurs through Bain straining [40] rather than through partial dislocation activity.

To verify the phase transition path and the energy barrier of the phase transformation, the energy landscape underlying the fcc-bcc-hcp phase transformation was evaluated using *ab initio* calculations [Fig. 3(e)]. During the calculations, the fcc structure ($a = 0.416$ nm) served as the initial state (Step 0), the bcc structure ($a = 0.328$ nm) was the first state (Step 8), and the hcp structure ($a = 0.293$ nm and $c = 0.484$ nm) was the final state (Step 16). As can be observed from the calculated energy curves, the energy of the hcp structure is located in a valley, which indicates that the hcp phase is stable. Although bcc-structured Ag has a high energy, it is located in a tiny valley. This implies that the bcc phase is metastable [3], which was also confirmed by our experimental observation that bcc Ag was often localized near the interface. Based on the *ab initio* calculations, it can be concluded that the phase transition should follow a Bain strain path [40,41] according to the change in the "principal axis" (see details in Figs. S5–S6 and Tables I–II [31]). As shown in Fig. S5(a) [31], corresponding to the fcc-bcc transformation of the Bain model, the continuous strain leads to an increase in the a/c ratio from 1 to $\sqrt{2}$ [see Fig. S5(c) and Table I [31]]. After the formation of the bcc phase, as shown in Fig. S6, further straining of the bcc structure led to the bcc-hcp transformation following the Bain model. The corresponding fcc, bcc, and hcp structures are shown in the inset of Fig. 3(d). Based on the *ab initio* calculations, the corresponding three-dimensional (3D) atomic models of fcc-, bcc-, and hcp-structured Ag [shown in the inset of Fig. 3(d)] were found to be consistent with our experimental results. Figures 3(g)–3(j) show the two-dimensional (2D) atomic models of the fcc, bcc, hcp, and re-oriented fcc phases obtained from the *ab initio* calculations.

We also conducted a series of compressive (Fig. S7 [31]) and tensile (Fig. 4 and Figs. S8–S11 [31]) loading experiments on Ag NWs with different orientations. The results of these tests show that the plasticity of ultrasmall NWs is governed by dislocation activity under tensile deformation, while phase transformation occurs under bending. The results are consistent with those of previous, conventional

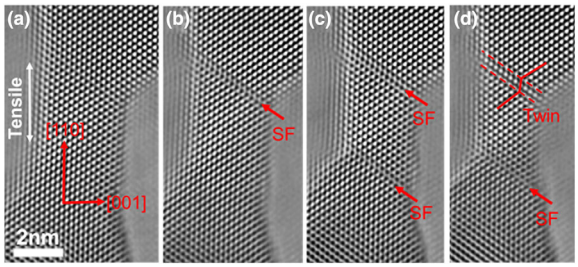

FIG. 4. An examples showing the plastic deformation of the ultrasmall NW governed by a partial dislocation resulting in stacking faults and deformation twins during tensile loading.

compression and tensile deformation experiments [24,42–45]. Our *in situ* atomic-scale results, together with those of previous compression and tensile deformation experiments and atomistic simulations, provide a comprehensive picture of the deformation mechanism of fcc metals. Under conventional compressive/tensile loading, the plasticity of metals is governed by dislocation activity and deformation twinning. However, during bending, phase transition is an important mechanism to accommodate the bending strain, at least for Ag NWs. Additionally, we provide direct evidence that deformation twinning can occur through continuous phase transition, which has seldom been reported.

Generally, even under extreme conditions, metals can access only one or two of the above-mentioned structures at room temperature. Our results show that bending can provide fcc-structured Ag with access to all three structures (fcc, hcp, and bcc) at room temperature. According to previous studies, the fcc-hcp transition can be realized through partial dislocation emission on alternating close-packed (111) planes. Interestingly, our *ab initio* calculations (Fig. S12 [31]) showed that the energy barrier of a partial-dislocation-induced fcc-hcp transition is lower than the Bain strain fcc-bcc-hcp path. The activation of the high-energy Bain strain path may be due to the following reasons: First, the inhomogeneous strain distribution likely makes the region at the bottom side of the bent NWs a confined domain (Fig. S13 [31]). Because this "confined domain" is ultra-small (with a size less than 2 nm), dislocation activity is suppressed [5,10]. Thus, this ultra-small-sized region can endure high stresses according to the principle of "smaller is stronger" [5,10], ultimately facilitating the fcc-bcc-hcp-fcc transformation. Second, the inhomogeneous bending strain makes dislocation activity unfavorable. The generation of plastic strain requires dislocation nucleation and glide through the NWs. For NWs undergoing conventional compressive/tensile deformation, the above-mentioned dislocation activity can easily occur because the strain distribution is relatively homogeneous. Whereas for a bent NW, the upper side of the central axis undergoes tensile strain, and the bottom side of the central axis undergoes compressive strain. This inhomogeneous strain is unfavorable for the nucleation and glide of dislocations in the NWs. Thus, in this case, plastic strain through dislocation activity is unfavorable. Third, bending can avoid early fracture initiation that easily occurs during tensile deformation, and can also sufficiently increase the strain energy to trigger the fcc-bcc-hcp-fcc transformation. This phase can accommodate a considerable amount of the strain energy and can consequently accommodate the bending strain.

In conclusion, an atomic-scale bending deformation mechanism of Ag NWs was investigated *in situ* using a homemade deformation device. It was shown that bending provides an effective way to provide fcc-structured Ag with access to fcc, bcc, and hcp structures at room temperature. The results also revealed a new deformation mechanism of NWs under bending strain, where an NW accommodates the bending strain through fcc-bcc-hcp-fcc phase transition. The results of this study advance our understanding of the deformation mechanism of small-sized fcc metals.

This work was supported by the Beijing Natural Science Foundation (Z180014) and the Beijing Outstanding Young Scientists Projects (BJJWZYJH012019100005018), the Natural Science Foundation of China (51771004, 12174014, 91860202, 51831004, U1930402) and "111" project (DB18015).

*These authors contributed equally to this work.
†Corresponding author.
wlh@bjut.edu.cn
‡Corresponding author.
xdhan@bjut.edu.cn

[1] Y. Chen, Z. C. Lai, X. Zhang, Z. X. Fan, Q. Y. He, C. L. Tan, and H. Zhang, Nat. Rev. Chem. **4**, 243 (2020).
[2] Z. X. Fan *et al.*, Nat. Commun. **6**, 6571 (2015).
[3] Z. A. Tian, R. S. Liu, C. X. Zheng, H. R. Liu, Z. Y. Hou, and P. Peng, J. Phys. Chem. A **112**, 12326 (2008).
[4] J. Sun, L. B. He, Y. C. Lo, T. Xu, H. C. Bi, L. T. Sun, Z. Zhang, S. X. Mao, and J. Li, Nat. Mater. **13**, 1007 (2014).
[5] L. H. Wang *et al.*, Nat. Commun. **4**, 2413 (2013).
[6] Y. Lu, S. D. Sun, Y. P. Zeng, Q. S. Deng, Y. H. Chen, Y. Z. Li, X. Y. Li, L. H. Wang, and X. D. Han, Mater. Res. Lett. **8**, 348 (2020).
[7] Q. Y. Lin, J. P. Liu, X. H. An, H. Wang, Y. Zhang, and X. Z. Liao, Mater. Res. Lett. **6**, 236 (2018).
[8] J. R. Greer and W. D. Nix, Phys. Rev. B **73**, 245410 (2006).
[9] J. R. Greer and J. T. M. De Hosson, Prog. Mater. Sci. **56**, 654 (2011).
[10] T. Zhu and J. Li, Prog. Mater. Sci. **55**, 710 (2010).
[11] H. Tang, K. W. Schwarz, and H. D. Espinosa, Acta Mater. **55**, 1607 (2007).
[12] S. Lee, J. Im, Y. Yoo, E. Bitzek, D. Kiener, G. Richter, B. Kim, and S. H. Oh, Nat. Commun. **5**, 3033 (2014).
[13] A. M. Leach, M. McDowell, and K. Gall, Adv. Funct. Mater. **17**, 43 (2007).
[14] Y. J. Gao, Y. L. Sun, X. B. Yang, Q. Sun, and J. W. Zhao, Mol. Simul. **42**, 220 (2016).

[15] R. Ramachandramoorthy, W. Gao, R. Bernal, and H. Espinosa, Nano Lett. **16**, 255 (2016).
[16] Y. Zhu, Q. Q. Qin, F. Xu, F. R. Fan, Y. Ding, T. Zhang, B. J. Wiley, and Z. L. Wang, Phys. Rev. B **85**, 045443 (2012).
[17] C. Deng and F. Sansoz, ACS Nano **3**, 3001 (2009).
[18] J. W. Wang, F. Sansoz, J. Y. Huang, Y. Liu, S. H. Sun, Z. Zhang, and S. X. Mao, Nat. Commun. **4**, 1742 (2013).
[19] H. Zheng, A. J. Cao, C. R. Weinberger, J. Y. Huang, K. Du, J. B. Wang, Y. Y. Ma, Y. N. Xia, and S. X. Mao, Nat. Commun. **1**, 144 (2010).
[20] F. Delogu, J. Phys. Chem. C **114**, 3364 (2010).
[21] J. Diao, K. Gall, and M. L. Dunn, Nat. Mater. **2**, 656 (2003).
[22] H. S. Park, K. Gall, and J. A. Zimmerman, Phys. Rev. Lett. **95**, 255504 (2005).
[23] W. W. Liang, M. Zhou, and F. J. Ke, Nano Lett. **5**, 2039 (2005).
[24] X. W. Gu, C. N. Loynachan, Z. X. Wu, Y. W. Zhang, D. J. Srolovitz, and J. R. Greer, Nano Lett. **12**, 6385 (2012).
[25] A. M. Nie and H. T. Wang, Mater. Lett. **65**, 3380 (2011).
[26] R. Thevamaran, C. Griesbach, S. Yazdi, M. Ponga, H. Alimadadi, O. Lawal, S. J. Jeon, and E. L. Thomas, Acta Mater. **182**, 131 (2020).
[27] B. S. Li, X. D. Wen, R. P. Li, Z. W. Wang, P. G. Clem, and H. Y. Fan, Nat. Commun. **5**, 4179 (2014).
[28] Y. G. Sun, W. G. Yang, Y. Ren, L. Wang, and C. H. Lei, Small **7**, 606 (2011).
[29] H. L. Zhao, M. Song, S. Ni, S. Shao, J. Wang, and X. Z. Liao, Acta Mater. **131**, 271 (2017).
[30] Y. J. Chen *et al.*, Acta Mater. **215**, 117112 (2021).
[31] See Supplemental Material at http://link.aps.org/supplemental/10.1103/PhysRevLett.128.015701 for additional details regarding the experiments and analysis, which includes Refs. [32–38].
[32] L. H. Wang *et al.*, Nat. Commun. **8**, 2142 (2017).
[33] L. H. Wang, K. Du, C. P. Yang, J. Teng, L. B. Fu, Y. Z. Guo, Z. Zhang, and X. D. Han, Nat. Commun. **11**, 1167 (2020).
[34] G. Henkelman, B. P. Uberuaga, and H. Jonsson, J. Chem. Phys. **113**, 9901 (2000).
[35] G. Kresse and J. Furthmuller, Comput. Mater. Sci. **6**, 15 (1996).
[36] J. P. Perdew, K. Burke, and M. Ernzerhof, Phys. Rev. Lett. **77**, 3865 (1996).
[37] G. Kresse and D. Joubert, Phys. Rev. B **59**, 1758 (1999).
[38] P. E. Blochl, Phys. Rev. B **50**, 17953 (1994).
[39] M. I. Novgorodova, A. I. Gorshkov, and V. Mokhov, Int. Geol. Rev. **23**, 485 (1981).
[40] E. C. Bain, Trans. AIME **70**, 25 (1924).
[41] P. Alippi, P. M. Marcus, and M. Scheffler, Phys. Rev. Lett. **78**, 3892 (1997).
[42] X. L. Wu, X. Z. Liao, S. G. Srinivasan, F. Zhou, E. J. Lavernia, R. Z. Valiev, and Y. T. Zhu, Phys. Rev. Lett. **100**, 095701 (2008).
[43] C. Chisholm, H. Bei, M. B. Lowry, J. Oh, S. A. S. Asif, O. L. Warren, Z. W. Shan, E. P. George, and A. M. Minor, Acta Mater. **60**, 2258 (2012).
[44] J. Y. Kim, D. C. Jong, and J. R. Greer, Acta Mater. **58**, 2355 (2010).
[45] C. R. Weinberger and W. Cai, Proc. Natl. Acad. Sci. U.S.A. **105**, 14304 (2008).